Creating traveling waves from standing waves from the gyrotropic paramagnetic properties of Fe^{3+} ions in a high-Q whispering gallery mode sapphire resonator

Karim Benmessai* and Michael Edmund Tobar†
School of Physics M013, University of Western Australia, 35 Stirling Highway, Crawley, Western Australia 6009, Australia

Nicholas Bazin, Pierre-Yves Bourgeois, Yann Kersalé, and Vincent Giordano
Institut FEMTO-ST, UMR 6174 CNRS, Université de Franche-Comté, 25044 Besançon, France
(Received 1 January 2009; published 27 May 2009)

We report observations of the gyrotropic change in magnetic susceptibility of the Fe^{3+} electron paramagnetic resonance at 12.037 GHz (between spin states $|1/2\rangle$ and $|3/2\rangle$) in sapphire with respect to the applied magnetic field. Measurements were made by observing the response of the high-Q whispering gallery doublet in a Hemex sapphire resonator cooled to 5 K. The doublets initially existed as standing waves at zero field and were transformed to traveling waves due to the gyrotropic response.

DOI: 10.1103/PhysRevB.79.174432 PACS number(s): 06.30.Ft, 76.30.−v, 84.40.Ik, 32.30.Bv

I. INTRODUCTION

Residual paramagnetic impurities in ultrapure Hemex sapphire crystals greatly influence the electromagnetic properties of the resonators cooled to near-liquid-helium temperature. For example, the electron paramagnetic resonance (EPR) of impurities such as Cr^{3+}, Ti^{3+}, and Mo^{3+} influences the temperature dependence, and allows frequency-temperature turnover (annulment) near liquid-helium temperature, which can vary between 2 and 10 K.[1–4] This phenomenon is vital in producing ultrastable frequencies for cryogenic sapphire oscillators[5–8] and the study of EPR in low-loss crystals has become an important topic of investigation.[9–12] More recently, it was shown that the small amount of residual Fe^{3+} ions (less than parts per million) are sufficient to create maser oscillations due to the zero-field three-level system between $|1/2\rangle$, $|3/2\rangle$, and $|5/2\rangle$ spin states.[13–15] This has allowed a different way to operate a cryogenic sapphire oscillator, where population inversion is created by pumping the spin states in the $|1/2\rangle$ transition to the $|5/2\rangle$ transition with a 31.3 GHz pump, and has the potential to operate with a frequency stability governed by the Schawlow-Townes noise limit[16] (sub-10^{-16} frequency stability).

In this work we show how the application of an axial magnetic field on a cryogenic sapphire resonator, with a mode tuned on the Fe^{3+} EPR, adds a gyrotropic component of magnetic susceptibility. This is achieved due to the very high-Q whispering gallery (WG) modes (on the order of 10^9) that are excited, which enables the discrimination of the two degenerate standing wave modes known as a doublet. Precision measurement of the frequency and Q factor of the doublet reveals an asymmetric response, which demonstrates that the susceptibility added by the magnetic field is predominately of gyrotropic origin and that the modes transform to traveling waves. Traveling waves are known to enhance the interaction between the pump radiation and the maser medium due to the elimination of standing wave nodes, and should be a way of generating greater output power in the respective solid-state maser.

II. WHISPERING GALLERY MODE FIELDS

To determine the electromagnetic fields of the mode under investigation we use a separation of variables technique, which has proven to be reliable for the approximate calculation of electromagnetic fields and properties of high-Q WG modes in low-loss sapphire resonators.[17,18] To calculate the gyrotropic properties we apply perturbation analysis on the nongyrotropic fields. The technique assumes that the resonator is a perfect cylinder of uniaxial anisotropy with the c axis aligned along the cylinder z axis as shown in Fig. 1.

For electromagnetic modes existing in nongyrotropic media with one or more azimuthal variations, m of 2π ($m>0$), two degenerate mode solutions exist (doublet) as orthogonal displaced standing wave solutions proportional to either $\cos(m\phi)$ or $\sin(m\phi)$. The degeneracy of the modes is lifted by a very small amount (only observable in high-Q systems) due to dielectric backscatter or other perturbations, which couple the counter clockwise (CCW) $e^{jm\phi}$ or clockwise (CW) $e^{-jm\phi}$ parts between the two doublet standing wave modes.[19–21] In gyrotropic media, the doublets have their degeneracy further modified in a nonreciprocal fashion, and the modes must transform to the traveling wave basis (rather than standing wave) with opposite elliptical polarization due

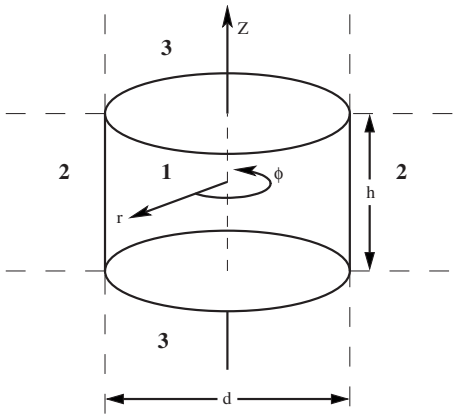

FIG. 1. Solution regions for separation of variables in cylindrical coordinates.

to the nonreciprocity imposed by the gyrotropic effect.[22,23]

In this work we observe gyrotropic effects on a quasi-transverse magnetic WG doublet pair, which is represented by the notation, $\mathrm{WGH}_{\pm m,n,p}$. Here n represents the number of radial zero crossings, p represents the number of axial zero crossings, and the "±" symbol represents the sense of the elliptical polarization of the doublets. For the fundamental $\mathrm{WGH}_{\pm m,0,0}$ mode family the E_z electric field is the dominant component and is symmetric along the z axis (around $z=0$). Given these conditions one can show that the solutions to Maxwell's equations yield (the time dependence $e^{j\omega t}$ is assumed):

$$E_{z1\pm} = A_{1\pm} e^{\pm jm\phi} \cos(\beta z) J_m(k_E r),$$

$$E_{z2\pm} = A_{2\pm} e^{\pm jm\phi} \cos(\beta z) K_m(k_{\mathrm{out}} r),$$

$$E_{z3\pm} = A_{3\pm} e^{\pm jm\phi} e^{-\alpha_E z} J_m(k_E r),$$

$$H_{z1\pm} = B_{1\pm} e^{\pm jm\phi} \sin(\beta z) J_m(k_H r),$$

$$H_{z2\pm} = B_{2\pm} e^{\pm jm\phi} \sin(\beta z) K_m(k_{\mathrm{out}} r),$$

$$H_{z3\pm} = B_{2\pm} e^{\pm jm\phi} e^{-\alpha_H z} J_m(k_H r). \quad (1)$$

To calculate the other components we apply the following Maxwell's relationships to the z components given in Eq. (1) in the regions 1–3 (derived from Maxwell's equations in cylindrical coordinates):

$$\left(k^2 + \frac{\partial^2}{\partial z^2}\right) H_{r\pm} = j\omega\varepsilon_\perp \varepsilon_0 \frac{1}{r}\frac{\partial E_{z\pm}}{\partial \phi} + \frac{\partial^2 H_{z\pm}}{\partial z\, \partial r}, \quad (2a)$$

$$\left(k^2 + \frac{\partial^2}{\partial z^2}\right) E_{\phi\pm} = j\omega\mu_0 \frac{\partial H_{z\pm}}{\partial r} + \frac{1}{r}\frac{\partial^2 E_{z\pm}}{\partial z\, \partial \phi}, \quad (2b)$$

$$\left(k^2 + \frac{\partial^2}{\partial z^2}\right) H_{\phi\pm} = -j\omega\varepsilon_\perp \varepsilon_0 \frac{1}{r}\frac{\partial E_{z\pm}}{\partial \phi} + \frac{\partial^2 H_{z\pm}}{\partial z\, \partial \phi}, \quad (2c)$$

$$\left(k^2 + \frac{\partial^2}{\partial z^2}\right) E_{r\pm} = -j\omega\mu_0 \frac{\partial H_{z\pm}}{\partial r} + \frac{1}{r}\frac{\partial^2 E_{z\pm}}{\partial z\, \partial r}. \quad (2d)$$

Here, $\varepsilon_{//}=11.349$ and $\varepsilon_\perp=9.272$ are the uniaxial permittivity components of sapphire cooled close to liquid-helium temperature (~5 K) parallel and perpendicular to the c axis, respectively.

The mode pair that we are interested in is the $\mathrm{WGH}_{\pm 17,0,0}$ inside a sapphire crystal of 50 mm in diameter and 30 mm in height at room temperature. Contraction from room temperature to 5 K is taken into account in the modeling by the factors of 0.999 27 along the z axis and 0.999 39 perpendicular to the z axis.[24–26] Matching boundary conditions with the same approximations as given in Ref. 18, we obtain the following values of the parameters, as shown in Table I; note that initially no gyrotropic effects are assumed (the effects are small and perturbation analysis suffices). This means the initial calculation of the "+" and "−" polarized modes are degenerate.

The parameters in Table I are independent of the elliptical polarization, and electromagnetic filling factors may be calculated from Eq. (3), which also turn out to be independent of elliptical polarization, and are shown in Table II.

$$p_{mi} = \frac{\int\int\int_{V_i} \mu_0 H_i^* H_i d\nu}{\int\int\int_V \mu_0 H^* H d\nu} p_{ei} = \frac{\int\int\int_{V_i} \varepsilon_0 E_i^* E_i d\nu}{\int\int\int_V \varepsilon(\nu) E^* E d\nu}. \quad (3)$$

Here i defines the component of the field and corresponding component of filling factor within the corresponding region of volume V_i. The normalization factor calculates the total field energy across all regions in the total volume of the resonator, V.

Note that the largest components of the field within the sapphire are E_z and H_r; this means that the dominant propagation is around the azimuth (Poynting theorem) as expected for a WG mode. Also, the three most dominant components (H_r, H_ϕ, and E_z), are that of a transverse magnetic mode with the H_ϕ component combining with the H_r to define the sense of the elliptical polarization. The amount of field in the vacuum surrounding the dielectric (regions 2 and 3) may be calculated by $1-p_{ez}-p_{er}-p_{e\phi}=0.006\,799\,54$ and $1-p_{mz}-p_{mr}-p_{m\phi}=0.082\,833\,2$, respectively.

To determine the sense of elliptical polarization we take a closer look at the solution of the dominant components for the "+" and "−" modes in region 1 (the sapphire dielectric), which are calculated by substituting Eqs. (1) into region 1

$$E_{z1+} = e^{jm\phi} \cos(\beta z)[-E_{z1o} J_m(k_E r)],$$

$$H_{r1+} = e^{jm\phi} \cos(\beta z)\left[H_{r1a}\frac{\partial J_m(k_H r)}{\partial r} + H_{r1b}\frac{J_m(k_E r)}{r}\right],$$

$$H_{\phi 1+} = je^{jm\phi} \cos(\beta z)\left[H_{\phi 1a}\frac{\partial J_m(k_H r)}{\partial r} + H_{\phi 1b}\frac{J_m(k_E r)}{r}\right],$$

$$E_{z1-} = e^{-jm\phi} \cos(\beta z)[E_{z1o} J_m(k_H r)],$$

$$H_{r1-} = e^{-jm\phi} \cos(\beta z)\left[H_{r1a}\frac{\partial J_m(k_H r)}{\partial r} + H_{r1b}\frac{J_m(k_E r)}{r}\right],$$

TABLE I. Calculated parameters from matching boundary conditions for the $\mathrm{WGH}_{\pm 17,0,0}$ mode pair.

Frequency ±	k_H	k_E	β	k_{out}	α_H	α_E
12.0305 GHz	717.707	802.952	103.866	760.709	841.609	j 229.754

TABLE II. Electromagnetic filling factors within sapphire dielectric (region 1) for the $WGH_{\pm 17,0,0}$ mode pair.

p_{ez1}	p_{er1}	$p_{e\phi 1}$	p_{mz1}	p_{mr1}	$p_{m\phi 1}$
0.970 906	0.003 429 36	0.018 864 7	0.002 926 8	0.835 142	0.079 097 7

$$H_{\phi 1-} = -je^{-jm\phi}\cos(\beta z)\left[H_{\phi 1a}\frac{\partial J_m(k_H r)}{\partial r} + H_{\phi 1b}\frac{J_m(k_E r)}{r}\right]. \tag{4}$$

Here, the solution requires $H_{r1a}=1.09\times10^{-7}E_{z1o}$, $H_{r1b}=1.82\times10^{-4}E_{z1o}$, $H_{\phi 1a}=1.86\times10^{-6}E_{z1o}$, and $H_{\phi 1b}=1.07\times10^{-5}E_{z1o}$. Thus, by inspection the polarization of the magnetic field for the CCW propagating mode is proportional to $e^{jm\phi}$ and has CCW elliptical polarization (+ mode) while the magnetic field for the CW propagating mode proportional to $e^{-jm\phi}$ has CW elliptical polarization (− mode).

III. GYROTROPIC REPRESENTATION

In this work we show that gyrotropic effects occur on the $WGH_{17,0,0}$ doublet pair when tuned within the Fe^{3+} EPR in the presence of a dc magnetic field. To calculate the gyrotropic nature we use the same notation as presented by Gurevich.[27] We assume the case of a weak magnetic response, which is true for our situation as we use the purest Hemex sapphire available, which has no more than the order of parts per million of residual impurity ions.[1,4,10,28] In this case the magnetic susceptibility added can be considered independent of the microwave field, i.e., only dependent on the applied dc field. The permeability added by the EPR response to the magnetic field in the axial direction is a tensor of the form:

$$\overleftrightarrow{\mu}(B) = \begin{bmatrix} \mu_\perp(B) & j\mu_a(B) & 0 \\ -j\mu_a(B) & \mu_\perp(B) & 0 \\ 0 & 0 & 1 \end{bmatrix}. \tag{5}$$

Thus, the change in permeability (or change in susceptibility) created by the response to the external field is given by the following:

$$\Delta\overleftrightarrow{\mu}(B) = \overleftrightarrow{\mu}(B) - \mu_0\overleftrightarrow{I} = \begin{bmatrix} \Delta\mu_\perp(B) & j\mu_a(B) & 0 \\ -j\mu_a(B) & \Delta\mu_\perp(B) & 0 \\ 0 & 0 & 0 \end{bmatrix}. \tag{6}$$

Here, $\overleftrightarrow{I}$ is the unitary matrix and in general the permeability components are complex.

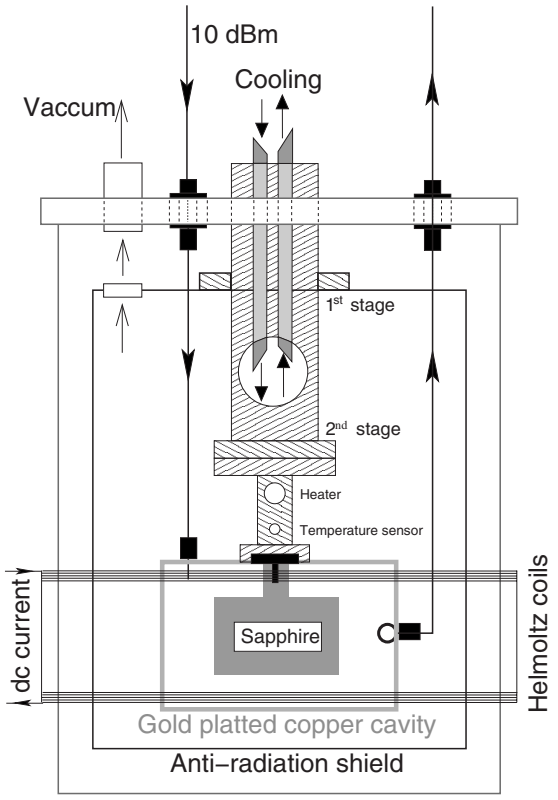

FIG. 2. The sapphire resonator was mounted in a gold plated copper cavity and measured in transmission with 10 dBm of incident power from a network analyzer. The dc magnetic field in the axial direction was applied by a Helmholtz coil pair system as shown above. The resonator was placed in vacuum and fixed on a cryocooler (PT 405) cold finger and cooled close to 5 K using a temperature control system.

IV. APPLICATION OF PERTURBATION THEORY

The typical value of susceptibility added by residual impurities is of the order 10^{-8}, thus we apply perturbation theory based on the fields calculated using separation of variables in Sec. III. Following the method in Gurevich, the change in complex frequency may be calculated from the change in complex permeability from,

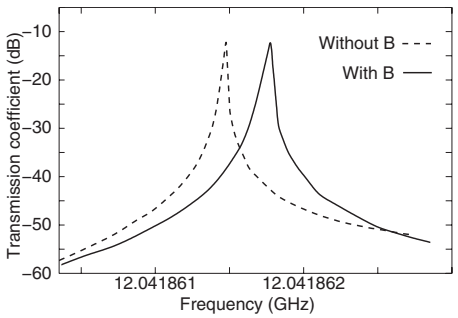

FIG. 3. Frequency, Q factor, and mode coupling were recorded using a network analyzer referenced to a hydrogen maser to avoid frequency drift of the network analyzer. For resonator 1 the coil's sensitivity is 4 G/A and 1 G/A for resonator 2.

TABLE III. Zero-field properties of the $WGH_{\pm 17,0,0}$ doublet in sapphire resonator number 1.

Mode (sapphire no. 1)	Frequency (GHz)	Q_0
Lower	12.023 984 181	3.5×10^8
Upper	12.023 994 100	13.8×10^8

TABLE IV. Zero-field properties of the $WGH_{\pm 17,0,0}$ doublet in sapphire resonator number 2.

Mode (sapphire no. 2)	Frequency (GHz)	Q_0
Lower	12.041 856 348	5.9×10^8
Upper	12.041 861 773	7.3×10^8

$$\frac{\Delta f_\pm}{f_\pm} = \frac{\int\int\int_{V_i} H_\pm^* \Delta\tilde{\mu} H_\pm d\nu}{\int\int\int_V \varepsilon(\nu) E_\pm^* E_\pm d\nu + \int\int\int_V \mu_0 H_\pm^* H_\pm d\nu}. \tag{7}$$

Here, f_0 is the unperturbed frequency (no gyrotropic effect) so that $\Delta f_\pm = f_\pm - f_0$, where $\Delta f_\pm / f_\pm$ is in general complex. In this work the complex fractional frequency is defined by $\Delta f_\pm / f_\pm = \Delta f_{\mathrm{Re}_\pm}/f_\pm + j\Delta f_{\mathrm{Im}_\pm}/f_\pm$, where the real part describes the frequency shift and the imaginary part describes the unloaded Q shift, where $Q_{B_\pm}^{-1} \approx 2\Delta f_{\mathrm{Im}_\pm}/f_\pm$. The total-mode-unloaded Q values ($Q_{0_\pm}$) is related to the zero-field-unloaded Q values ($Q_{ZF_\pm}$) and the shift due to the magnetic field by $Q_{0_\pm}^{-1} = Q_{ZF_\pm}^{-1} + Q_{B_\pm}^{-1}$. For the above model the complex permeability added by the magnetic field is of the form $\Delta\mu_\perp = \Delta\mu'_\perp - j\Delta\mu''_\perp$ and $\mu_a = \mu'_a - j\mu''_a$. Substituting the complex permeability into Eq. (6), and then Eq. (6) into Eq. (7) along with the unperturbed fields, the following sensitivities with respect to the permeability are calculated for the $WGH_{\pm 17,0,0}$ doublet:

$$\frac{\Delta f_{\mathrm{Re}+}}{f_+} = -0.457176(\Delta\mu'_\perp - 0.10485\mu'_a) = -0.457176\Delta\mu'_{\mathrm{eff}+},$$

$$\frac{\Delta f_{\mathrm{Re}-}}{f_-} = -0.457176(\Delta\mu'_\perp + 0.10485\mu'_a) = -0.457176\Delta\mu'_{\mathrm{eff}-},$$

$$\frac{\Delta f_{\mathrm{Im}+}}{f_+} = 0.457176(\Delta\mu''_\perp - 0.10485\mu''_a) = 0.457176\Delta\mu''_{\mathrm{eff}+} = \frac{1}{2Q_{B+}},$$

$$\frac{\Delta f_{\mathrm{Im}-}}{f_-} = 0.457176(\Delta\mu''_\perp + 0.10485\mu''_a) = 0.457176\Delta\mu''_{\mathrm{eff}-} = \frac{1}{2Q_{B-}}. \tag{8}$$

The nonreciprocity of the two modes is highlighted by Eq. (8), which shows that the "–" and "+" modes are dependent on different effective permeability $\Delta\mu_{\mathrm{eff}_\pm} = \Delta\mu'_{\mathrm{eff}_\pm} - j\Delta\mu''_{\mathrm{eff}_\pm}$ (both real and imaginary).

The magnetization model of Gurevich predicts $\mu'_\perp$ and μ''_a to be of the same sign. Thus, given that both modes tune up in frequency with the magnetic field, the – or CW mode must be the mode with the greatest tuning coefficient. According to the model the mode should also be accompanied with a decreasing Q factor, while the + or CCW mode increases its Q factor. This is indeed what is observed in Sec. V, where two resonators are analyzed, and the values of $\Delta\mu'_\perp$, μ'_a, $\Delta\mu'_\perp$, and μ'_a are calculated as a function of the magnetic field.

V. EXPERIMENTAL RESULTS

Hemex sapphire crystals are known to have Fe^{2+} impurities in the crystal. To convert these ions to Fe^{3+} the crystals need to be annealed in an oxygen environment.[29] The resulting electron spin resonance (ESR) exhibits a zero-field ESR

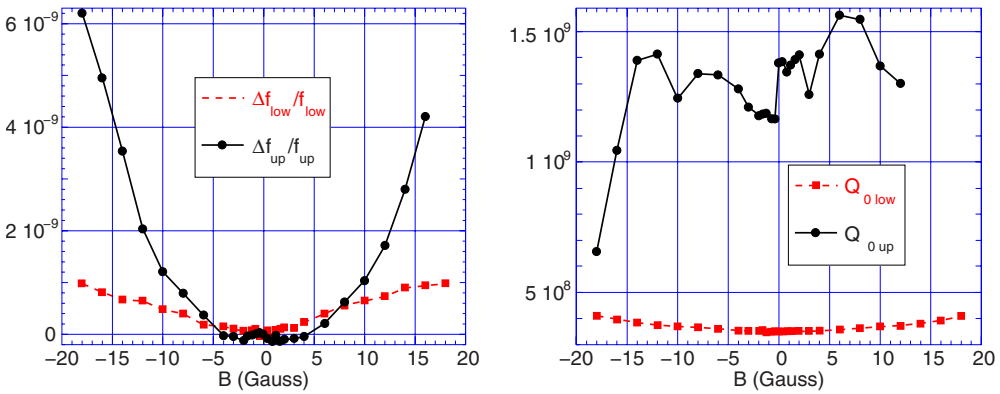

FIG. 4. (Color online) Left: measured fractional frequency shift for the $WGH_{\pm 17,0,0}$ lower and upper doublet modes as a function of applied axial magnetic field for sapphire No. 1 (Table III). Right: corresponding measured unloaded Q factor.

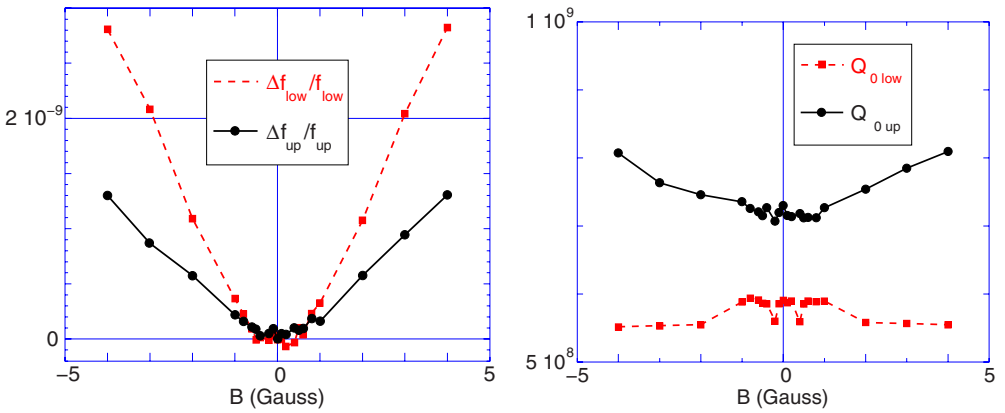

FIG. 5. (Color online) Left: measured fractional frequency shift for the $WGH_{\pm 17,0,0}$ lower and upper doublet modes as a function of applied axial magnetic field for sapphire No. 2 (Table IV). Right: corresponding measured unloaded Q factor.

between the $|1/2\rangle$ and $|3/2\rangle$ spin states at 12.037 GHz with a 27 MHz bandwidth.[14–16] The crystal resonators are nominally 50 mm in diameter and 30 mm in height; for such a resonator the $WGH_{\pm 17,0,0}$ doublet pair is tuned inside the ESR bandwidth, with a predicted frequency from the separation of variable technique of 12.03 GHz. In this work we report on the properties of two crystals, which were annealed. Measurements were taken on a crystal, which was not annealed; however, no measurable effects with respect to the magnetic field were observed. The experimental setup of the cryogenically cooled system with a variable external magnetic field is shown in Fig. 2.

The Q factors and frequencies of the two $WGH_{\pm 17,0,0}$ doublet modes were recorded as a function of the magnetic field for two separate sapphire resonators using a network analyzer in transmission. A typical recording of the transmission coefficient with and without the magnetic field on is shown in Fig. 3.

With zero field applied to the crystals the following parameters in Tables III and IV were measured. The doublet modes were already separated in frequency at zero field due to other nongyrotropic perturbations.[19,20,30] The modes are labeled as upper (subscript up) and lower (subscript low) for the higher and lower frequency-tuned modes. The frequency shift and unloaded Q factor of the upper and lower modes were measured as a function of the magnetic field, and are shown in Figs. 4 and 5 for the two resonators.

From the properties present in Figs. 4 and 5, it is straightforward to determine the polarizations of the modes. The − CW-polarized mode has a larger effective permeability with respect to the magnetic field and should thus tune at a greater rate. The same mode should also increase its effective loss tangent at the same time. Thus, for sapphire no. 1 the − mode is identified as the upper mode and the + CCW mode as the lower. It is the reverse situation for sapphire no. 2 as the lower mode is the − mode and the upper is the +. After this identification, Eq. (9) may be used to solve for the real and imaginary permeabilities. The solutions lead to the following equations

$$\Delta\mu_{\perp}' = -1.09367\left(\frac{\Delta f_{\mathrm{Re}-}}{f_{-}} + \frac{\Delta f_{\mathrm{Re}+}}{f_{+}}\right),$$

$$\Delta\mu_{\perp}'' = 1.09367\left(\frac{1}{Q_{B-}} + \frac{1}{Q_{B+}}\right),$$

$$\mu_{a}' = -10.4305\left(\frac{\Delta f_{\mathrm{Re}-}}{f_{-}} - \frac{\Delta f_{\mathrm{Re}+}}{f_{+}}\right), \tag{9}$$

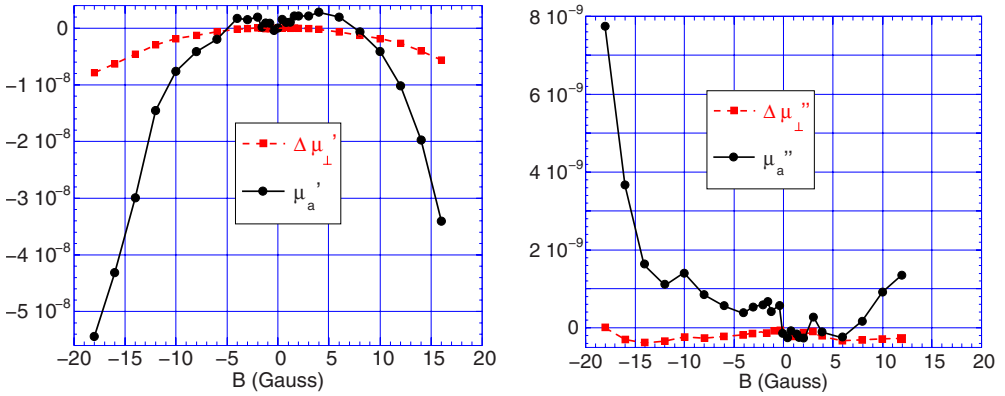

FIG. 6. (Color online) Left: real permeability components as a function of applied axial magnetic field for sapphire No. 1. Right: corresponding imaginary components. Note, the gyrotropic response is larger in both cases.

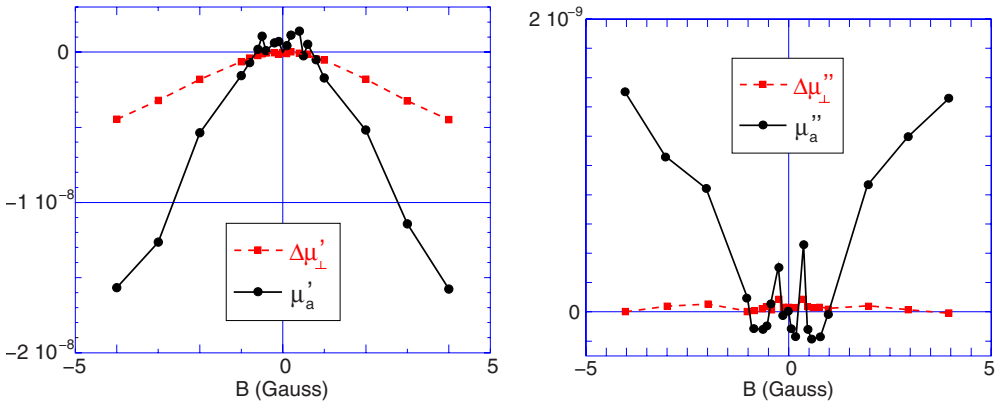

FIG. 7. (Color online) Left: real permeability components as a function of applied axial magnetic field for sapphire No. 2. Right: corresponding imaginary components. Note, the gyrotropic response is larger in both cases.

$$\mu_a'' = 10.4305\left(\frac{1}{Q_{B-}} + \frac{1}{Q_{B+}}\right).$$

Thus, from Eq. (9) and the data of Figs. 4 and 5, the change in complex permeability with respect to the magnetic field may be calculated and plotted in Figs. 6 and 7.

It is clear that the gyrotropic susceptibility added by the magnetic field is larger than the nongyrotropic component for both real and imaginary terms.

VI. TRAVELING WAVES

Coupled-mode theory is used to show that standing waves are converted to traveling waves. Previous analysis has shown that in high-Q systems perturbations, including backscatter happens due to the dielectric and other perturbations such as probes, and will cause the WG doublet to have its degeneracy lifted.[19,21,31] Coupled modes in tuneable high-Q sapphire resonators have been studied in detail previously.[32,33] The lifting of the degeneracy is caused by reactive coupling through the electromagnetic fields (strong coupling), which creates a bandgap between the modes. The frequency of the upper and lower modes with respect to a linear tuning parameter, x, are in general given by Eqs. (10).

$$\frac{f_{\text{up/low}}(x)}{f_0} = 1 \pm \sqrt{k^2x^2 + \Delta^2/4},$$

$$\frac{f_+(x)}{f_0} = 1 + kx \quad \frac{f_-(x)}{f_0} = 1 - kx. \tag{10}$$

Here the frequencies of the traveling waves f_+ and f_- depend linearly on the tuning parameter x, with a tuning coefficient of $\pm k$, respectively, an idealized diagram with respect to coupled-mode theory with $k=1/2$, is shown in Fig. 8. When the two modes have the same frequency, i.e., $x=0$ the mode separation due to the strong coupling is $f_{\text{up}}/f_0 - f_{\text{low}}/f_0 = \Delta$, which defines the strength of the coupling and the band-gap width.

The data represented in Figs. 4 and 5 show the mode frequencies tuning as a function of the magnetic field. The magnetic field tunes the frequencies due to the tuning of the EPR; however the tuning is nonlinear. Given that the nongyrotropic response of the EPR to the magnetic field should be in the linear regime, as the magnetic fields are relatively small[34] we may define the average frequency shift of the two modes as an effective linear tuning parameter, such that $x = B/|B|(f_{\text{up}} + f_{\text{low}})/2f_0$. Figures 9 and 10 show the differential shift between the two modes as a function of x (ignoring the initial mode splitting). The differential shift according to Eq. (10) will be of the form $(f_{\text{up}} - f_{\text{low}})/2f_0 = \sqrt{k^2x^2 + \Delta^2/4}$, and may be fitted to the experimental data to calculate the coupling parameter, Δ, between the traveling waves.

The ESR is inhomogenously broadened so the interaction will be with the spin packet of closest frequency in both sapphires. Sapphire 2 has a lower threshold of about 0.6 G compared to sapphire 1 with 4 G. The threshold value basically corresponds to the value of the magnetic field that the standing waves are transformed to traveling waves and to the point where the mode responds linearly to tuning parameter x with the value of k for the tuning coefficient. The threshold

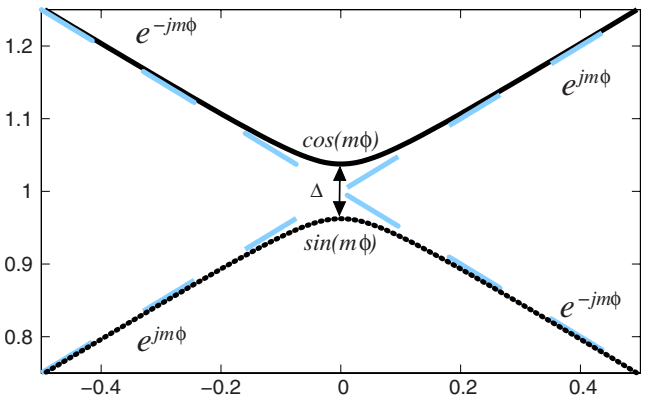

FIG. 8. (Color online) Normal-mode frequencies versus tuning parameter, x, with $k=1/2$ and $\Delta=0.1$ as given by Eq. (10). The top solid curve is the upper-tuned mode f_{up}/f_0 while the bottom solid curve is the lower-tuned mode f_{low}/f_0. The noncoupled modes in the traveling wave basis $f_\pm/f_0$ are given by the dashed lines. When the modes are detuned they behave as traveling waves, when they are tuned the modes interact and are mixed, and are best described by standing waves [$\cos(m\phi)$ and $\sin(m\phi)$]. The extent of the transition region depends on the strength of the coupling.

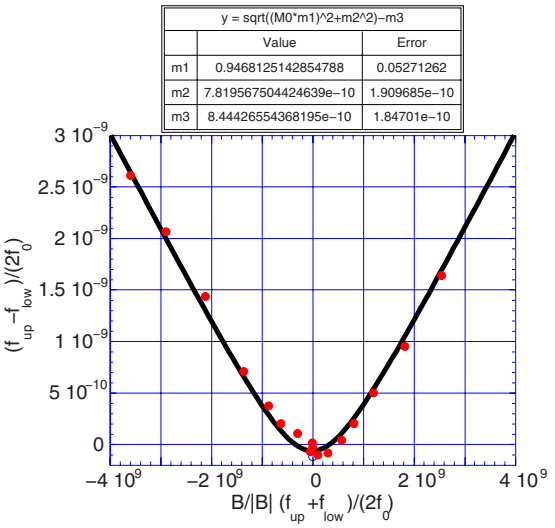

FIG. 9. (Color online) Fractional differential-mode frequency shift versus common-mode frequency shift for sapphire No. 1. The curve fit gives the coupling parameter $(m2)$ of $\Delta=7.8(1.9)\times10^{-10}$ and coefficient $(m1)$ $k=0.95(0.05)$.

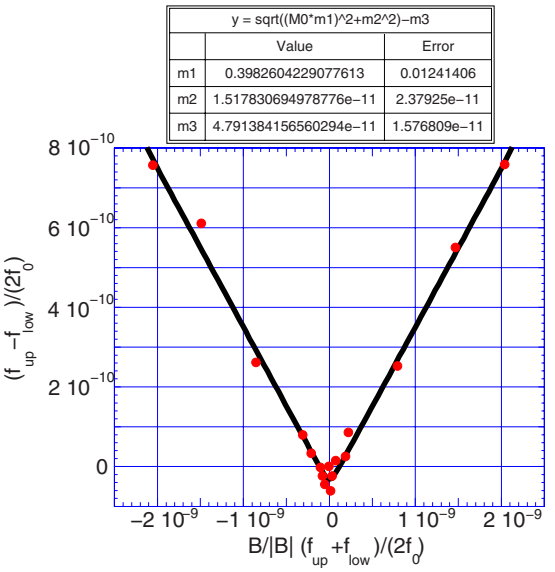

FIG. 10. (Color online) Fractional differential-mode frequency shift versus common-mode frequency shift for sapphire No. 2. The curve fit gives the coupling parameter $(m2)$ of $\Delta=1.5(2.4)\times10^{-11}$ and coefficient $(m1)$ $k=0.40(0.01)$.

magnetic field value also correlates with the value of the coupling strength between the traveling waves with the higher value demanding a stronger coupling. Thus, the more tightly coupled, the traveling waves the stronger the magnetic field threshold that is required to transform them into traveling waves.

The doublet splitting at zero field is of the order of 10^{-7}, which is more than 2 orders of magnitude than the coupling parameter measured in this work. However, this splitting is most likely due to the nonperfect cylindrical radius. Once the modes transform to standing waves they sample orthogonal space along the azimuthal dimension and will "see" a different effective radius. Only a difference of 2.5 μm over the 25 mm radius is required to account for this. The hypothesis is supported by the fact that the tolerance of the radial circumference in the machining process given by the manufacture is ±50 μm.

VII. CONCLUSION

The contribution to the magnetic susceptibility (or permeability) of the EPR of Fe^{3+} ions in sapphire at 12.03 GHz (between spin states $|1/2\rangle$ and $|3/2\rangle$) with respect to a dc axial magnetic field has been measured from precision measurements of Q factor and frequency of a WG mode doublet pair at 4.2 K. The form of the susceptibility was shown to be predominantly gyrotropic causing nonreciprocal response of the measured resonant modes. We showed that the gyrotropic response converted the standing waves to traveling waves due to the nonreciprocal response.

ACKNOWLEDGMENTS

This work was supported by the Centre National d'Études Spatiales (CNES), the Agence Nationale pour la Recherche (ANR), the Australian Research Council (ARC), and traveling support from FAST program from Egide and the International Science Linkages program from DEST.

*kbenmess@cyllene.uwa.edu.au
†mike@physics.uwa.edu.au

[1] S. K. Jones, D. G. Blair, and M. J. Buckingham, Electron. Lett. **24**, 346 (1988).
[2] R. P. Kovacich, A. G. Mann, and D. G. Blair, J. Phys. D **30**, 3146 (1997).
[3] A. N. Luiten, A. G. Mann, and D. G. Blair, J. Phys. D **29**, 2082 (1996).
[4] A. G. Mann, A. J. Giles, D. G. Blair, and M. J. Buckingham, J. Phys. D **25**, 1105 (1992).
[5] P. Y. Bourgeois, F. Lardet-Vieudrin, Y. Kersale, N. Bazin, M. Chaubet, and V. Giordano, Electron. Lett. **40**, 605 (2004).
[6] A. J. Giles, A. G. Mann, S. K. Jones, D. G. Blair, and M. J. Buckingham, Physica B **165**, 145 (1990).
[7] J. G. Hartnett, C. R. Locke, E. N. Ivanov, M. E. Tobar, and P. L. Stanwix, Appl. Phys. Lett. **89**, 203513 (2006).
[8] C. R. Locke *et al.*, Rev. Sci. Instrum. **79**, 051301 (2008).
[9] J. G. Hartnett and M. E. Tobar, in *Frequency Measurement and Control*, Vol. 79 of Topics in Applied Physics, edited by A. N. Luiten (Springer-Verlag, Berlin, 2001), pp. 67–91.
[10] J. G. Hartnett, M. E. Tobar, J. M. Le Floch, J. Krupka, and P. Y. Bourgeois, Phys. Rev. B **75**, 024415 (2007).

[11] J. G. Hartnett, M. E. Tobar, and J. Krupka, J. Phys. D **34**, 959 (2001).
[12] J. G. Hartnett, M. E. Tobar, A. G. Mann, E. N. Ivanov, J. Krupka, and R. Geyer, IEEE Trans. Ultrason. Ferroelectr. Freq. Control **46**, 993 (1999).
[13] K. Benmessai, P. Y. Bourgeois, Y. Kersale, N. Bazin, M. E. Tobar, J. G. Hartnett, M. Oxborrow, and V. Giordano, Electron. Lett. **43**, 1436 (2007).
[14] P. Y. Bourgeois, N. Bazin, Y. Kersalé, V. Giordano, M. E. Tober, and M. Oxborrow, Appl. Phys. Lett. **87**, 224104 (2005).
[15] P. Y. Bourgeois, M. Oxborrow, M. E. Tobar, N. Bazin, Y. Kersalé, V. Giordano, Int. J. Mod. Phys. B **20**, 1606 (2006).
[16] K. Benmessai, D. L. Creedon, M. E. Tobar, P. Y. Bourgeois, Y. Kersale, and V. Giordano, Phys. Rev. Lett. **100**, 233901 (2008).
[17] M. E. Tobar and A. G. Mann, IEEE Trans. Microwave Theory Tech. **39**, 2077 (1991).
[18] P. Wolf, M. E. Tobar, S. Bize, A. Clairon, A. N. Luiten, and G. Santarelli, Gen. Relativ. Gravit. **36**, 2351 (2004).
[19] M. L. Gorodetsky, A. D. Pryamikov, and V. S. Ilchenko, J. Opt. Soc. Am. B **17**, 1051 (2000).
[20] T. J. Kippenberg, S. M. Spillane, and K. J. Vahala, Opt. Lett. **27**, 1669 (2002).
[21] D. S. Weiss, V. Sandoghdar, J. Hare, V. Lefèvre-Seguin, J. -M. Raimond, and S. Haroche, Opt. Lett. **20**, 1835 (1995).
[22] J. Krupka, P. Blondy, D. Cros, P. Guillon, and R. G. Geyer, IEEE Trans. Microwave Theory Tech. **44**, 1097 (1996).
[23] J. Krupka and R. G. Geyer, IEEE Trans. Microwave Theory Tech. **32**, 1924 (1996).
[24] J. Krupka, K. Derzakowski, A. Abramowicz, M. E. Tobar, and R. G. Geyer, IEEE Trans. Microwave Theory Tech. **47**, 752 (1999).
[25] J. Krupka, K. Derzakowski, M. Tobar, J. Hartnett, and R. G. Geyer, Meas. Sci. Technol. **10**, 387 (1999).
[26] M. E. Tobar, J. Krupka, E. N. Ivanov, and R. A. Woode, J. Phys. D **30**, 2770 (1997).
[27] A. G. Gurevich, *Ferrites at Microwave Frequencies* (State Press for Physicomathematical Literature, Moscow, 1960).
[28] M. E. Tobar and J. G. Hartnett, Phys. Rev. D **67**, 062001 (2003).
[29] F. Benabid, M. Notcutt, V. Loriette, L. Ju, and D. G. Blair, J. Phys. D **33**, 589 (2000).
[30] P. Y. Bourgeois and V. Giordano, IEEE Trans. Microwave Theory Tech. **53**, 3185 (2005).
[31] A. Mazzei, S. Gotzinger, L. de S. Menezes, G. Zumofen, O. Benson, and V. Sandoghdar, Phys. Rev. Lett. **99**, 173603 (2007).
[32] M. Tobar, J. Phys. D **26**, 2022 (1993).
[33] M. Tobar and D. Blair, IEEE Trans. Ultrason. Ferroelectr. Freq. Control **39**, 1582 (1991).
[34] L. S. Kornienko and A. M. Prokhorov, Sov. Phys. JETP **13**, 1120 (1961).